THE JOURNAL OF PHYSICAL CHEMISTRY A

Article

pubs.acs.org/JPCA

Selective Photoinduced Ligand Exchange in a New Tris−Heteroleptic Ru(II) Complex

Bryan A. Albani, Christopher B. Durr, and Claudia Turro*

Department of Chemistry and Biochemistry, The Ohio State University, Columbus, Ohio 43210, United States

Supporting Information

ABSTRACT: The complex *cis*-$[Ru(biq)(phen)(CH_3CN)_2]^{2+}$ (**1**, biq = 2,2′-biquinoline, phen = 1,10-phenathroline) displays selective photosubstitution of only one CH_3CN ligand with a solvent molecule upon irradiation with low energy light ($\lambda_{irr} \geq 550$ nm), whereas both ligands exchange with $\lambda_{irr} \geq 420$ nm. In contrast, $[Ru(phen)_2(CH_3CN)_2]^{2+}$ (**2**) and $[Ru(biq)_2(CH_3CN)_2]^{2+}$ (**3**) exchange both CH_3CN ligands with similar rates upon irradiation with a broad range of wavelengths. The photolysis of **1** in the presence of pyridine (py) results in the formation of the intermediate *cis*-$[Ru(biq)(phen)(py)(MeCN)]^{2+}$, which was isolated and characterized by X-ray crystallography, revealing that the CH_3CN positioned *trans* to the phen ligand is more photolabile than that positioned *trans* to the biq ligand when irradiated with low energy light. These results are explained using the calculated stabilities of the two possible products, together with the molecular orbitals involved in the lowest energy excited state.

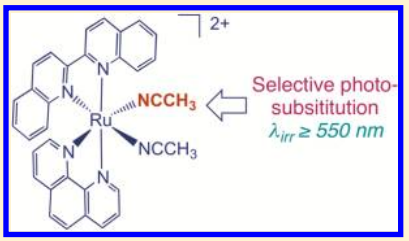

INTRODUCTION

Understanding the photochemistry of transition metal complexes is essential to the development of areas that include solar energy conversion, photocatalysis, and photochemotherapy (PCT).[1−15] These processes are initiated by the absorption of a photon by the molecule, placing it in an excited state that is able to undergo reactions that are not accessible from the ground state.[15−17] Ruthenium(II) complexes are of particular interest due to their success as sensitizers in dye sensitized solar cells,[5,15] as well as their potential as PCT agents.[18−24] In addition, many of these Ru(II) complexes have the ability to undergo excited state ligand substitution.[25−27]

The broadly accepted model for the mechanism of photoinduced ligand exchange in complexes with lowest-energy ^{3}MLCT (metal-to-ligand charge transfer) excited states relies on the thermal population of the reactive ^{3}LF (ligand field) dd state(s) from the lower-lying ^{3}MLCT state(s).[28−39] The population of the ^{3}LF state(s) places electron density on the e_g-type orbitals with Ru−L σ^* character, thus resulting in ligand dissociation.[28−39] Accordingly, the energy gap between the ^{3}MLCT and the ^{3}LF states has been shown to have a pronounced effect on the quantum yield of ligand exchange when the low-lying MLCT state is excited selectively.[34−36] Moreover, direct excitation of the LF state(s) with higher energy light results in a significant increase in the photoreactivity.[31−33]

The exploration of the photochemistry of Ru(II) complexes possessing monodentate CH_3CN ligands such as $[Ru(bpy)(CH_3CN)_4]^{2+}$ (bpy = 2,2′-bipyridine) and $[Ru(bpy)_2(CH_3CN)_2]^{2+}$ revealed efficient ligand exchange of the CH_3CN ligand with a coordinating solvent or with excess halide upon irradiation with visible light.[40,41] It was shown that ligand exchange occurred in a stepwise manner and that the quantum yield for the exchange of the second CH_3CN ligand is ∼2-fold lower than that of the first CH_3CN ligand.[40,41] Moreover, in $[Ru(bpy)(CH_3CN)_4]^{2+}$, which possesses four potential sites for exchange, only the axial CH_3CN ligands undergo stepwise substitution with water upon irradiation.[40] This reactivity provides an important synthetic tool for the preparation of new *trans* Tris−heteroleptic Ru(II) complexes, as well as PCT agents with photolablile ligands that can function in hypoxic environments without the need for oxygen.[19−24]

In the present work, the asymmetric complex $[Ru(biq)(phen)(CH_3CN)_2]^{2+}$ (**1**, Figure 1) (biq = 2,2′-biquinoline, phen = 1,10-phenathroline) was synthesized and characterized, and its photochemical properties were investigated. The results were compared to those of the symmetric complexes $[Ru(phen)_2(CH_3CN)_2]^{2+}$ (**2**, Figure 1) and $[Ru(biq)_2(CH_3CN)_2]^{2+}$ (**3**, Figure 1). Each of the complexes **1**−

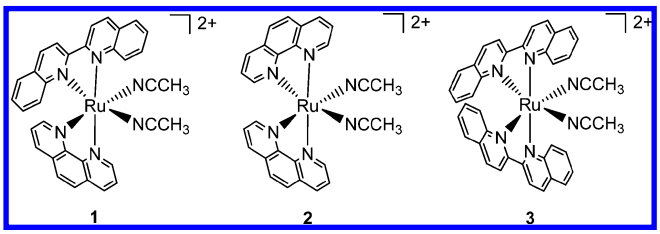

Figure 1. Schematic representation of the molecular structures of **1**−**3**.

Special Issue: Terry A. Miller Festschrift

Received: August 27, 2013
Revised: October 14, 2013
Published: October 14, 2013

dx.doi.org/10.1021/jp4085684 | J. Phys. Chem. A 2013, 117, 13885−13892

3 possesses two potentially photolabile CH_3CN ligands; however, unlike 2 and 3, one CH_3CN ligand of 1 is preferentially substituted upon irradiation. The monosubstituted intermediate generated following photolysis in pyridine was isolated and characterized to ascertain which CH_3CN ligand was exchanging. The work presented herein provides a greater understanding of photoinduced ligand exchange for the design of future systems with improved properties.

EXPERIMENTAL SECTION

Materials. $RuCl_3{\cdot}3H_2O$ and 2,2′-biquinoline (biq) were purchased from CP Laboratories and Acros Organic, respectively, and were used without further purification. Ascorbic acid, 1,10-phenanthroline (phen), potassium hexafluorophosphate, and ammonium hexafluorophosphate were purchased from Sigma-Aldrich and used as received. All solvents used were purchased from commercial sources and used without further purification unless otherwise specified. The complexes $Ru(phen)Cl_4$,[42] $[Ru(phen)(CH_3CN)_4](PF_6)_2$,[40] and $Ru(phen)_2Cl_2$[43] were prepared according to literature procedures.

Instrumentation. The ^1H NMR spectra of all complexes were recorded using a Bruker 400 MHz DPX ultrashield system. Electronic absorption spectroscopy was carried out using a Hewlett-Packard 8453 diode array spectrometer, emission spectra were obtained on a Horiba Fluormax-4 spectrometer, and electrochemical studies were performed on a BAS CV-50W voltammetric analyzer. Photolysis and quantum yield experiments were carried out using a 150 W Xe short arc lamp (USHIO) in a Milliarc lamp housing unit (PTI) powered by a LPS-220 power supply (PTI) equipped with a LPS-221 igniter (PTI). The desired wavelength range was attained using bandpass filters (Thorlabs, fwhm ∼ 10 nm) or 3 mm thick (2 mm for 610 nm) long-pass filters (CVI Melles Griot).

$[Ru(biq)(phen)(CH_3CN)_2](PF_6)_2$ (1). $[Ru(phen)(CH_3CN)_4](PF_6)_2$ (0.040 g, 0.0544 mmol) and 2,2′-biquinoline (0.014 g, 0.0542 mmol) were dissolved in 6 mL of DMF:CH_3CN (5:1). The yellow solution was stirred and degassed for 5 min with N_2, and was then refluxed for 15 h during which time a gradual color change from yellow to orange and then to light red was observed. The reddish orange solid was precipitated by the addition of 100 mL of H_2O and was filtered on a glass frit by vacuum filtration. The solid was dissolved in 20 mL of a CH_3CN:H_2O mixture (50:50) and heated under reflux for 4 h, and 5 mL of a concentrated solution of NH_4PF_6 was added to the solution while still hot. The mixture was slowly cooled to room temperature and then placed in an ice bath. A reddish orange solid precipitated and was filtered on a glass frit by vacuum filtration (0.015 g, 31% yield). ^1H NMR (400 MHz, $(CD_3)_2CO$) δ 10.36 (dd, 1H, ^3J = 5.2 Hz, ^4J = 1.2 Hz), 9.25 (d, 1H, ^3J = 8.9 Hz), 9.08 (m, 2H), 8.96 (dd, 1H, ^3J = 8.2 Hz, ^4J = 1.2 Hz), 8.79 (d, 1H, ^3J = 8.8 Hz), 8.57 (m, 2H), 8.42 (m, 2H), 8.2 (m, 3H), 8.03 (t, 1H, ^3J = 7.4 Hz), 7.87 Hz (m, 3H), 7.73 (m, 1H), 7.57 (t, 1H, ^3J = 3.5 Hz), 7.34 (t, 1H, ^3J = 4.2 Hz), 2.71 (s, 3H), 2.30 (s, 3H). Elem. anal. calcd. for $[Ru(biq)(phen)(CH_3CN)_2](PF_6)_2{\cdot}3(C_2H_5)_2O{\cdot}2H_2O$: C, 48.8%; N, 7.42%; H, 4.97%. Found: C, 48.10%; N, 6.62%; H, 4.25%.

$[Ru(phen)_2(CH_3CN)_2](PF_6)_2$ (2). $Ru(phen)_2Cl_2$ (0.055 g, 0.10 mmol) was dissolved in 20 mL of a mixture of CH_3CN and H_2O (50:50, v:v) and was refluxed for 4 h. The solution was slowly cooled to room temperature, and the solvent was evaporated to dryness by blowing with air. The remaining yellow solid was dissolved in 15 mL of H_2O washed with 5 aliquots of 20 mL of CH_2Cl_2 until the organic layer was clear. CH_3CN (10 mL) was added to the aqueous layer, and the mixture was refluxed for 1 h. A saturated solution of NH_4PF_6 in water (5 mL) was added to the solution while hot; the mixture was allowed to cool slowly to room temperature and was then placed in an ice bath. A yellow solid precipitated, and the powder was collected by vacuum filtrations and washed with 20 mL of diethyl ether (0.053 g, 62% yield). ^1H NMR (400 MHz, $(CD_3)_2CO$) δ 10.05 (dd, 2H, ^3J = 5.3 Hz, ^4J = 1.2 Hz), 9.05 (dd, 2H, ^3J = 8.3 Hz, ^4J = 1.3 Hz), 8.64 (dd, 2H, ^3J = 7.1 Hz, ^4J = 1.4 Hz), 8.46 (d, 2H, ^3J = 9.1 Hz), 8.37 (m, 2H), 8.32 (d, 2H, ^3J = 9.0 Hz), 8.09 (dd, 2H, ^3J = 5.3 Hz, ^4J = 1.2 Hz), 2.45 (s, 6H). Elem. anal. calcd. for $[Ru(phen)_2(CH_3CN)_2](PF_6)_2$: C, 40.3%; N, 10.1%; H, 2.66%. Found: C, 40.3%; N, 9.96%; H, 2.74%.

$Ru(biq)_2Cl_2$. $Ru(biq)_2Cl_2$ was prepared using a modification of the synthesis reported by Kubow et al.[44] $RuCl_3{\cdot}H_2O$ (0.18 g, 0.67 mmol), 2,2′-biquinoline (0.37 g, 1.5 mmol), and LiCl (0.087 g, 2.1 mmol) were dissolved in 7 mL of *N*,*N*-dimethylformamide. The solution was stirred until all solids dissolved, was degassed with N_2 for 5 min, and was then refluxed for 6 h turning a dark green color. The reaction mixture was slowly cooled to room temperature and pipetted dropwise into 500 mL of stirring H_2O, forming a green/blue precipitate that was collected by vacuum filtration. The solid was dissolved in CH_2Cl_2 forming a dark green solution, and then filtered to get rid of any remaining solid that did not dissolve. The green filtrate was washed 5 times with 20 mL of H_2O and then evaporated to a minimal amount of CH_2Cl_2. An excess of diethyl ether was added to the green CH_2Cl_2 solution, resulting in the formation of a green precipitate that was collected by vacuum filtration (0.22 g, 48% yield).

$[Ru(biq)_2(CH_3CN)_2](PF_6)_2$ (3). A procedure analogous to that for 2 was followed but using $Ru(biq)_2Cl_2$ (0.055 g, 0.080 mmol) as the starting material, which resulted in the isolation of a maroon powder (0.043 g, 54% yield). ^1H NMR (400 MHz, $(CD_3)_2CO$) δ 8.75 (d, 2H ^3J = 8.7 Hz), 8.42 (d, 2H, ^3J = 8.2 Hz), 8.34 (d, 2H, ^3J = 8.1 Hz), 8.20 (m, 4H), 8.01 (m, 4H), 7.92 (d, 2H, ^3J = 8.0 Hz), 7.46 (t, 2H, 7.1 Hz), 6.80 (m, 4H), 2.46 (s, 6H). Elem. anal. calcd. for $[Ru(biq)_2(CH_3CN)_2](PF_6)_2{\cdot}C_2H_6O$: C, 48.7%; N, 8.52%; H, 3.07%. Found: C, 48.9%; N, 8.15%; H, 3.52%.

Methods. ^1H NMR spectroscopy was performed in $(CD_3)_2CO$ (acetone-d_6), CD_3CN, or C_5D_5N (py-d_5), and all resonances were referenced to the residual protonated solvent peak. In the photolysis experiments monitored by ^1H NMR spectroscopy in CD_3CN or py-d_5, the intensities of the peaks were integrated relative to an internal standard of benzene (25 μL). The chloride salt of each complex was used for experiments performed in H_2O, which were obtained using an ion exchange column. The stationary phase was composed of Amberlite IRA-410 ion-exchange resin prepared by soaking in 1 M HCl at 50 °C for 3 days, and methanol was used as the eluent. Emission was measured at both room temperature and 77 K in CH_3CN in 1 × 1 cm^2 quartz cuvettes using an excitation wavelength corresponding to the maximum of the MLCT absorption for each complex. Cyclic voltammetry experiments were performed in a three-electrode cell with a Pt working electrode, a Pt wire auxiliary electrode, and a saturated Ag/AgCl reference electrode. The samples were dissolved in distilled CH_3CN containing 0.1 M tetrabutylammonium hexafluorophosphate as the supporting electrolyte and

dx.doi.org/10.1021/jp4085684 | J. Phys. Chem. A 2013, 117, 13885−13892

bubbled with N_2 for 10 min prior to each measurement. The cyclic voltammetry data was recorded at a scan rate of 100 mV/s, and ferrocene was added to each sample after the measurement as an internal standard (+0.40 V vs SCE in CH_3CN).[45] Elemental analysis was performed by Atlantic Microlab Inc.

The quantum yields (Φ) for photoinduced ligand exchange of the first CH_3CN in H_2O were measured for complexes **1** and **3** with 500 and 550 nm irradiation wavelengths using the appropriate bandpass filters.[46] The moles of complex reacted was quantitated using electronic absorption spectroscopy by monitoring the decrease in MLCT absorption maximum of each complex as a function of irradiation time (moles reacted/s) at early irradiation times, and Reinecke's salt was used as an actinometer to determine the intensity (Einstein/s) of the Xe arc lamp at the corresponding wavelengths.[46,47] The Φ for the photoinduced ligand exchange of the second CH_3CN ligand was measured for **1** using 400 and 550 nm irradiation wavelengths using the appropriate bandpass filters monitoring the decrease in the MLCT absorption peak of the monoaqua intermediate, **4**.[46]

Crystals suitable for single X-ray diffraction were grown for **1** and $[Ru(biq)(phen)(CH_3CN)(py)]^{2+}$ (**6**) by slow vapor diffusion. An ∼2 mg sample was dissolved in a mixture of CH_3CN, THF, and acetone (0.25, 0.10, and 0.25 mL, repectively) in a small vial and inserted into a larger vial partially filled with ether, which was sealed and placed in the freezer, resulting in red rods over a period of 2 weeks.

Single crystals of both **1** and **6** were isolated as block-like dark red crystals and handled under a pool of fluorinated oil. Examination of the diffraction pattern was done on a Nonius Kappa CCD diffractometer with Mo Kα radiation. All work was done at 150 K using an Oxford Cryosystems Cryostream Cooler. Data integration was done with Denzo, and scaling and merging of the data was done with Scalepack.[48] The structures were solved by the direct methods program in SHELXS-97.[49] Full-matrix least-squares refinements based on F^2 were performed in SHELXL-97,[49] as incorporated in the WinGX package.[50] For each methyl group, the hydrogen atoms were added at calculated positions using a riding model with U(H) = 1.5Ueq (bonded carbon atom). The rest of the hydrogen atoms were included in the model at calculated positions using a riding model with U(H) = 1.2Ueq (bonded atom). Neutral atom scattering factors were used and include terms for anomalous dispersion.[51] Compound **6** was disordered in several locations, and was composed of a mixture of compounds. A description of how compound **6** was modeled can be found embedded in the CIF file in the Supporting Information.

Calculations were performed with density functional theory (DFT) using the Gaussian 09 program.[52] The B3LYP[53−55] functional along with the 6-31G* basis set for H, C, and N[56] and the SDD energy consistent pseudopotentials were used for Ru.[57] Model compounds were generated by replacing the methyl groups with hydrogen atoms on the acetonitrile groups and named **1**′, **2**′, and **3**′ for complexes **1**, **2**, and **3**, respectively. Optimization of full geometries was carried out with the respective programs, and orbital analysis was performed in Gaussview version 3.09.[58] Following optimization of the molecular structures, frequency analysis was performed to ensure the existence of local minima on the potential energy surfaces. Electronic absorption singlet to singlet transitions were calculated using time-dependent DFT (TD-DFT) methods with the polarizable continuum model (PCM) that mimicked the solvation effect of CH_3CN in Gaussian 09.[59] Singlet−triplet transitions were also calculated to generate difference density plots of the lowest energy triplet excited states.

RESULTS AND DISCUSSION

Electronic Absorption, Emission, and Electrochemistry. The ^{1}MLCT absorption maxima of **1**, **2**, and **3** in CH_3CN are observed at 497 nm (ε = 7800 M^{-1} cm^{-1}), 420 nm (ε = 10 200 M^{-1} cm^{-1}), and 535 nm (ε = 7900 M^{-1} cm^{-1}), respectively. As expected, the sequential replacement of the phen ligands in **2** for biq in **1** and **3** results in a stepwise red shift in the lowest energy MLCT absorption maximum (Figure S5, Supporting Information).[60] A similar trend is observed in the polypyridyl complexes $[Ru(phen)_3]^{2+}$, $[Ru(phen)_2(biq)]^{2+}$, and $[Ru(phen)(biq)_2]^{2+}$ with ^{1}MLCT maxima at 450, 523, and 551 nm in methanol, respectively.[16,60] In addition to the Ru → biq ^{1}MLCT absorption in **1**, a shoulder at ∼410 nm arising from the Ru → phen ^{1}MLCT transition in the complex is apparent, which is at a position similar to that of **2**.[60] Very weak emission is observed for **1** (λ_{exc} = 500 nm) and **3** (λ_{exc} = 535 nm) at room temperature and **2** is not emissive (λ_{exc} = 420 nm); however, relatively strong luminescence was detected for all three complexes at 77 K (Figures S6−S10, Supporting Information), as is typical for related complexes.[60]

Cyclic voltammetry reveals quasi-reversible oxidation events, $E_{1/2}(Ru^{3+/2+})$, at +1.51, +1.45, and +1.55 V vs SCE for **1**, **2**, and **3**, respectively, in CH_3CN. The similarity among the three potentials points at a metal-centered process, as is typical of Ru(II)−polypyridyl complexes.[16] Quasi-reversible reduction waves in **2** are observed at −1.39 and −1.55 V vs SCE, at potentials similar to the ligand-centered reduction processes reported previously for the complex.[61] As expected, these waves are shifted to −0.77 and −1.04 V vs SCE in **3**, since the electrons are localized on the biq ligands with a more extended π-system as compared to phen. The reduction potentials measured for **3** are comparable to those published for related Ru(II) complexes containing the same ligand, including $[Ru(biq)(bpy)_2](PF_6)_2$ and $[Ru(biq)_2(bpy)](PF_6)_2$ with $E_{1/2}(Ru^{2+/+})$ = −0.97 and −0.89 V vs SCE, respectively.[62] In the asymmetric complex **1**, the two reversible reduction waves are observed at −0.91 and −1.45 V vs SCE, assigned to reduction of the biq ligand at the more positive potential, followed by reduction of the phen ligand.

Photochemistry. The photoreactivity of **1**−**3** was evaluated by monitoring the changes to the electronic absorption and ^{1}H NMR spectra as a function of irradiation time. All three complexes possess photolabile CH_3CN ligands with photochemistry that can be accessed with $\lambda_{irr} \geq$ 550 nm for **1**, $\lambda_{irr} \geq$ 455 nm for **2**, and $\lambda_{irr} \geq$ 610 nm for **3**. Complexes **1**−**3** are inert to ligand substitution in the dark at room temperature under similar experimental conditions. For the symmetrical complexes **2** and **3**, one resonance is observed in CD_3CN corresponding to the methyl protons of both bound acetonitrile ligands at 2.22 and 2.28 ppm, respectively. During the photolysis of **2** in CD_3CN with $\lambda_{irr} \geq$ 455 nm, the resonance at 2.22 ppm decreases with increasing irradiation time, while a peak at 1.96 ppm corresponding to free CH_3CN in CD_3CN increases in intensity at the same rate. The photolysis of **3** in CD_3CN with $\lambda_{irr} \geq$ 610 nm yields similar results with the decrease of the peak at 2.28 ppm with the concomitant increase of the free CH_3CN resonance at 1.96 ppm. The intensity of the peak corresponding to free CH_3CN at 1.96 ppm integrates to two ligands at the end

dx.doi.org/10.1021/jp4085684 | J. Phys. Chem. A 2013, 117, 13885−13892

of the photolysis for both **2** and **3** in CD_3CN, indicative that both CH_3CN ligands in **2** and **3** are exchanged (Figures S11 and S12, Supporting Information). It should be noted that, because of the electronic equivalence of CH_3CN and CD_3CN, the ^{1}H NMR resonance of bound CH_3CN ligands does not shift from those in **2** and **3** to that in the corresponding monosubstituted intermediate. Moreover, no shifts are observed in the aromatic region as the reaction progresses.

The changes to the ^{1}H NMR spectrum of **1** upon irradiation in CD_3CN using benzene as an internal integration standard are shown in Figure 2 ($\lambda_{irr} \geq 455$ nm). The CH_3CN ligands of

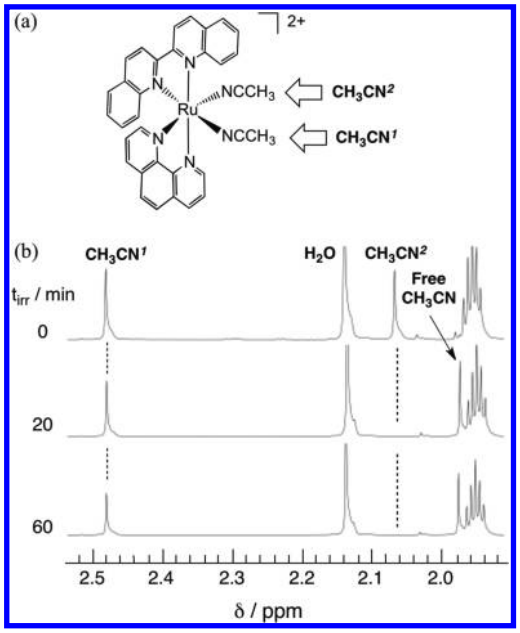

Figure 2. (a) Molecular structure of **1** with labeled CH_3CN ligands and (b) changes to the ^{1}H NMR spectrum of **1** in CD_3CN as a function of irradiation time ($\lambda_{irr} \geq 455$ nm).

1 are inequivalent, resulting in two resonances of equal integration at 2.53 and 2.12 ppm, labeled CH_3CN^1 and CH_3CN^2 in Figure 2a, respectively. Figure 2b shows that the resonance corresponding to CH_3CN^2 decreases at a faster rate than that of CH_3CN^1 upon irradiation in CD_3CN; the former disappears within 20 min of photolysis, while a significant portion (~75%) of the latter is still present after 60 min of irradiation. Because the disappearance of the peaks corresponding to bound CH_3CN ligands is concomitant with the increase of that associated with free CH_3CN at 1.96 ppm, the observed reactivity can be ascribed to the photoinduced ligand exchange with the CD_3CN solvent. The differences in photoinduced ligand exchange among **1**–**3** are illustrated in Figure S12 (Supporting Information), which shows that the substitution of the two CH_3CN ligands in **2** and **3** is complete in 5–60 min. In contrast, the photosubsitution of one CH_3CN ligand for CD_3CN in **1** is accomplished in ≤5 min, but the second CH_3CN ligand does not exchange up to 180 min of irradiation (Figure S12, Supporting Information).

The photolysis of **1** in H_2O ($\lambda_{irr} \geq 550$ nm) results in a decrease of the ^{1}MLCT band at 494 nm and the appearance of a peak with a maximum at 518 nm (Figure 3). The isosbestic points observed at 444 and 506 nm for the process are indicative of the formation of a single species, assigned as the monoaqua complex, *cis*-$[Ru(bpy)(biq)(CH_3CN)(H_2O)]^{2+}$, **4**.

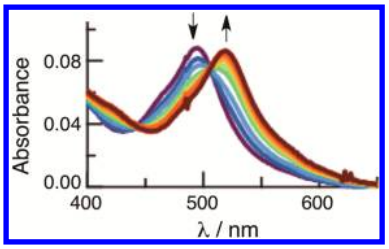

Figure 3. Changes to the electronic absorption spectrum of **1** (10 μM) in H_2O upon irradiation for 0–20 min ($\lambda_{irr} \geq 550$ nm).

The red shift of the MLCT maximum from **1** to **4** is similar to that previously reported between $[Ru(bpy)_2(CH_3CN)_2]^{2+}$ and $[Ru(bpy)_2(CH_3CN)(H_2O)]^{2+}$.[41] Continued irradiation with $\lambda_{irr} \geq 550$ nm results in negligible spectral changes and only at very long irradiation times, with the growth of a small shoulder at ~560 nm apparent after 3 h associated with the formation of a small amount of $[Ru(biq)(phen)(H_2O)_2]^{2+}$ (**5**). In contrast, when **1** is irradiated in H_2O with higher energy light, $\lambda_{irr} \geq 420$ nm, the formation of **5** is complete within 6 h. The 2192 cm^{-1} red-shift of the MLCT band observed from **1** to **5** is of the same magnitude as that reported between $[Ru(bpy)_2(CH_3CN)_2]^{2+}$ and $[Ru(bpy)_2(H_2O)_2]^{2+}$, 3121 cm^{-1}.[41]

It is evident in Figure 3 that irradiation of complex **1** in H_2O for 20 min ($\lambda_{irr} \geq 550$ nm) results in a well-defined absorption peak with a maximum at 518 nm, attributed to the monoaqua intermediate **4**, with negligible spectral changes with continued irradiation with this wavelength. However, when **4** is further irradiated with higher energy light ($\lambda_{irr} \geq 420$ nm), the bis-aqua species, **5**, is formed after 3 h (Figure S14, Supporting Information). The monoaqua intermediate **4**, produced by the photolysis of **1** in H_2O ($\lambda_{irr} \geq 550$ nm, Figure 3) is stable in the dark for up to 6 h at room temperature (Figure S15, Supporting Information).

In contrast to the results described with respect to **1**, irradiation of **2** ($\lambda_{irr} \geq 455$ nm, Figure 4a) and **3** ($\lambda_{irr} \geq 610$ nm,

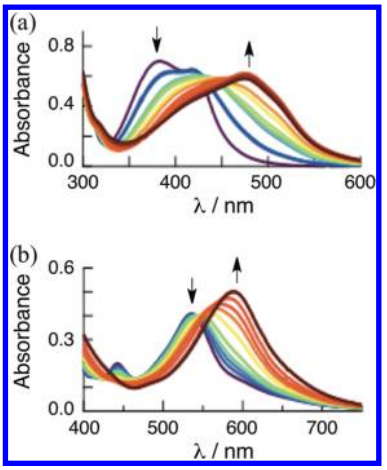

Figure 4. Irradiation of (a) 50 μM **2** ($\lambda_{irr} \geq 420$ nm, 0–90 min) and (b) 60 μM **3** ($\lambda_{irr} \geq 610$ nm, 0–120 min) in H_2O.

Figure 4b) results in complete conversion to the corresponding bis-aqua species. The intermediate peak corresponding to the monoaqua species associated with each complex is nearly unidentifiable (Figure 4), in agreement with the ^{1}H NMR photolysis data in CD_3CN (Figures S11 and S12, Supporting Information). These results lead to the conclusion that in **2** and

dx.doi.org/10.1021/jp4085684 | J. Phys. Chem. A 2013, 117, 13885–13892

3 both CH_3CN ligands exchange relatively easily, whereas in **1** one of the CH_3CN ligands is significantly more photolabile than the other.

The quantum yields for the first ligand exchange of **1** in H_2O to generate **4** with 500 and 550 nm irradiation, $\Phi_{500}^{1\rightarrow4}$ and $\Phi_{550}^{1\rightarrow4}$, were measured to be 0.26(1) and 0.140(5), respectively. These values are similar to those obtained for the formation of the monoaqua species from **3**, Φ_{500} = 0.24(1) and Φ_{550} = 0.150(8), as well as from **2**, Φ_{400} = 0.22(1). It should be noted that, as expected from the higher energy LF states in **2**, 400 nm light is required to obtain a similar quantum yield in this complex to those measured for **1** and **3** with 500 nm light. However, the quantum yields measured for the exchange of the remaining CH_3CN ligand from **4** to generate the bis-aqua complex **5** were significantly lower, $\Phi_{400}^{4\rightarrow5}$ = 0.0045(1) and $\Phi_{550}^{4\rightarrow5}$ = 0.0014(5). These results differ from those for systems such as $[Ru(bpy)(CH_3CN)_4]^{2+}$ and $[Ru(bpy)_2(CH_3CN)_2]^{2+}$ for which the quantum yield of the second photoinduced CH_3CN ligand exchange is approximately half the value of the first.[40,41] This comparison points to a selective ligand exchange in **1** that is not present in the symmetric complexes **2** and **3**.

In order to unequivocally assign which CH_3CN ligand of **1** is more photolabile, a photolysis intermediate was isolated and its structure was determined by X-ray crystallography. A mixture of pyridine (py) and CH_3CN (50:50, v:v) was used as the solvent rather than H_2O because py is a stronger coordinating ligand than H_2O, such that a more stable photolysis product was expected. In order to ensure the formation of the monosubstituted intermediate, a 550 nm bandpass filter was used, and the sample was irradiated until no additional changes in the absorption spectrum were apparent following the shift of the MLCT peak from 497 to 523 nm accompanied by a change in color from orange to red. After the photolysis was complete, the solution was concentrated and the $[Ru(phen)(biq)(CH_3CN)(py)]^{2+}$ (**6**) product was precipitated by the addition of ether. Slow evaporation of a solvent mixture of acetone, THF, and CH_3CN and diethyl ether resulted in red crystals suitable for X-ray diffraction, and the resulting ORTEP diagram is shown in Figure 5. It is evident from the two different views of the structure of **6** shown in Figure 5 that the py exchanged with the CH_3CN ligand positioned *trans* to the phen ligand (CH_3CN^2 in Figure 2a) with 80% occupancy clearly indicated that this is a more photolabile ligand in complex **1**. For the remaining 20% occupancy, both CH_3CN ligands were solved to be replaced by pyridine and the overall structure is a result of cocrystallization.

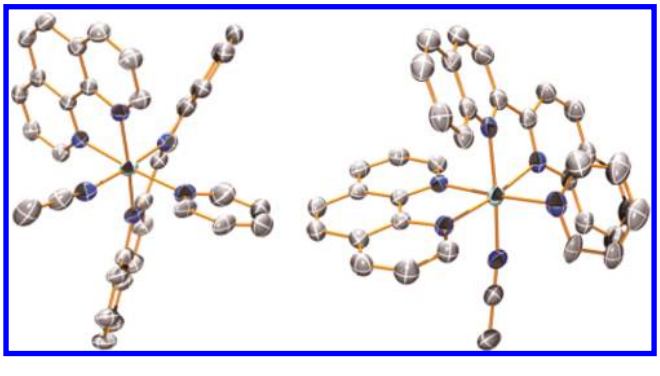

Figure 5. ORTEP plots of two different perspectives of PF_6^- salt of the monosubstituted intermediate **6** (ellipsoids drawn at 50% probability).

In order to confirm that the crystal structure of **6** accurately depicts the intermediate in solution, the photolysis ($\lambda_{irr} \geq 550$ nm) of complex **1** was carried out in deuterated pyridine (py-d_5) and was followed by ^1H NMR spectroscopy (Figure S16, Supporting Information). Upon irradiation up to 20 min, the two resonances corresponding to each bound CH_3CN ligand at 2.35 and 2.75 ppm decrease in intensity, with the concomitant growth of resonances at 2.95 and 1.84 ppm which integrate to 3H each. The former correspond to the remaining bound CH_3CN ligand in the monosubstituted intermediate, $[Ru(biq)(phen)(CH_3CN)(py\text{-}d_5)]^{2+}$, and the latter to free CH_3CN in py-d_5. Further irradiation results in a decrease in the 2.95 ppm peak of the intermediate and an increase in free CH_3CN resonance to form the bis-substituted product, $[Ru(biq)(phen)(py\text{-}d_5)_2]^{2+}$. The appearance of only one resonance associated with the intermediate indicates that only one of the bound CH_3CN ligands exchanges first, followed by the second, making the crystal structure of **6** shown in Figure 5 an accurate representation of the monosubstituted species.

CALCULATIONS

In order gain further understanding of the selective ligand photosubstitution of **1**, density functional theory (DFT) calculations were performed. The highest occupied molecular orbitals (HOMOs) of all three complexes, **1′**−**3′**, are calculated to be localized on the d-orbitals of the metal, as is typical of Ru(II)−diimine complexes.[1−4] The LUMO (lowest unoccupied molecular orbital) of **1′** exhibits electron density on the biq ligand and the LUMO+1 is localized on phen (Figure 6), as expected from the ease of reduction of biq relative to phen. When analyzing the unoccupied orbitals in **2′** and **3′**, the LUMOs are delocalized over both equivalent aromatic ligands of each complex, phen and biq, respectively.

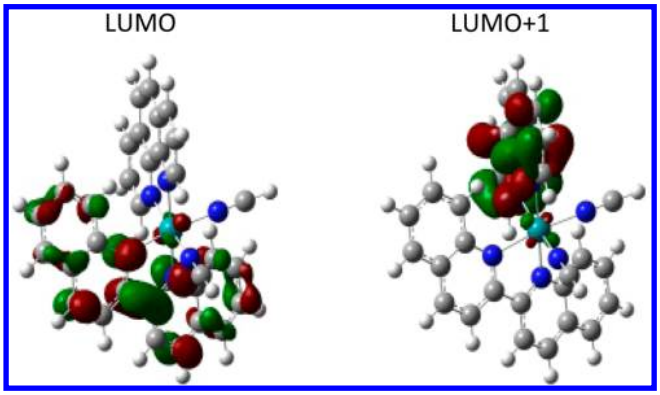

Figure 6. Electronic density plots of the calculated LUMO and LUMO +1 of **1′** (isovalue = 0.04).

Time-dependent DFT (TD-DFT) calculations reveal that the lowest vertical singlet excited states of **1′** and **3′** possess a significant contribution, ∼95%, from HOMO → LUMO transitions but low oscillator strengths, with maxima at 476 nm (f = 0.0002) and 496 nm (f = 0.0008), respectively (Tables S2−S4, Supporting Information). More intense absorption bands are predicted at 443 nm (f = 0.0646) for **1′** and at 475 nm (f = 0.1015) for **3′**, calculated to possess 67% and 94% contribution from HOMO-1 → LUMO transitions, respectively. The lowest energy vertical singlet excited states of **2′** are

dx.doi.org/10.1021/jp4085684 | J. Phys. Chem. A 2013, 117, 13885−13892

calculated at 396 nm (81% HOMO → LUMO+1, f = 0.0024) and at 395 nm (91% HOMO → LUMO, f = 0.0093). It should be noted that the lowest energy electronic transitions predicted are slightly blue-shifted relative to the experimental MLCT maxima, as is typical for DFT calculations.[63]

In order to understand the selective ligand exchange in **1**, the electron density of the orbitals with greatest contribution to the lowest energy excited state need to be considered, the HOMO and the LUMO. In the lowest energy singlet excited state, electron density is removed from the HOMO, which possesses a bonding interaction between the metal d-orbital and the CH_3CN ligand positioned *trans* to the phen ligand (Figure S17, Supporting Information). Therefore, the HOMO is involved in π-back bonding with CH_3CN, and removal of an electron from this MO is expected to weaken the bond. The LUMO of **1′** is localized on the π^* orbital of the biq ligand; placing electron density in this orbital is expected to strengthen the π-bond to the CH_3CN positioned *trans* to biq. Moreover, it has been reported that placing additional electron density on the bidentate ligand in the MLCT state of Re(I)−carbonyl complexes, such as in $[Re(bpy)(CO)_3(PR_3)]^+$, results in photoinduced ligand dissociation of the CO ligand positioned *cis* to bpy.[64] Similarly, selective photoinduced ligand exchange of the axial ligands in $[Ru(bpy)(CH_3CN)_4]^{2+}$ and $[Ru(tpy)(CH_3CN)_3]^{2+}$ was observed, where the CH_3CN ligands *trans* to the diimine, for which the π-backbonding is strengthened, do not exchange, but those positioned *cis* to the bpy or tpy ligand, respectively, are photolabile.[22,40] Since the LUMOs of **2′** and **3′** are delocalized equally over both diimine ligands, this selectivity is not observed. Furthermore, a greater amount of energy is required to populate the $Ru(t_{2g})$ → phen(π^*) MLCT singlet excited state in **1′** than the $Ru(t_{2g})$ → biq(π^*) MLCT singlet excited state (Table S2, Supporting Information). This could be a factor in the enhanced selectivity using lower energy light in which only the $Ru(t_{2g})$ → biq(π^*) state is accessed, yielding ligand loss of the CH_3CN *trans* to the phen ligand, while higher energy light results in an increased rate for both CH_3CN ligands due to the direct population of the $Ru(t_{2g})$ → phen(π^*) state.

It should also be noted that the lowest energy triplet state of **1′** resulting from the vertical transition from the minimized singlet ground state was calculated to be ^{3}MLCT Ru → biq in nature, similar to the lowest energy singlet excited state. The electron density difference plot for this ^{3}MLCT state is shown in Figure S18 (Supporting Information), along with those of **2′** and **3′**.

Additionally, the photoinduced ligand exchange is expected to occur via a dissociative mechanism,[16,25−33] such that the ligand exchange in **1** should proceed through a five-coordinate intermediate to produce the monosubstituted product, **4**.[41] Optimization of the five-coordinate species, $[Ru(biq)(phen)(HCN)]^{2+}$, starting from a trigonal bipyramidal geometry results in a distorted square pyramidal geometry (Figure S19, Supporting Information) with an open site for coordination positioned *trans* to the phen ligand. This result is consistent with the observation of the intermediate **6** (Figure 5), where the CH_3CN ligand *trans* to phen was photosubstituted. In addition, both possible monosubstitued products were optimized, with py *trans* to phen and *trans* to biq. When the py replaced the CH_3CN *trans* to the phen ligand, the overall energy was more stable by 11 kJ/mol relative to that *trans* to the biq, such that the former is thermodynamically favored (Figure S18, Supporting Information). It should be noted that the ^{3}MLCT excited states of **1**−**3** may be viewed as 17-electron species. Ground state ligand substitution in $M(CO)_6$ (M = Cr, Mo, W) complexes is believed to undergo ligand exchange through an associative mechanism.[65,66] In contrast, both associateive and dissociative mechanisms were reported for d^6 octahedral complexes of Ru(II) and Rh(III).[67] In addition, a recent study showed that in Ru(II)−polypyridyl complexes the mechanism of ligand substitution in the ground state changes from associative to dissociative with increasing steric bulk of the ligands.[68] Because the quantum yield of photoinduced ligand exchange is relatively independent of steric bulk in these complexes,[67] it is likely that the excited state reaction proceeds via a dissociative pathway as previously reported.[25−33]

CONCLUSIONS

The series of Ru(II) complexes **1**−**3** possess two CH_3CN ligands in a *cis* disposition and undergo photodinduced ligand exchange with solvent or coordinating molecules in solution when irradiated with visible light. Selective CH_3CN ligand exchange takes place in the asymmetric complex **1** with low energy irradiation ($\lambda_{irr} \geq 550$ nm), where only one of the ligands is photolabile. This selectivity is not observed in the symmetric complexes **2** and **3**. A crystal structure of the PF_6^- salt of the monosubstituted intermediate $[Ru(biq)(phen)(CH_3CN)(py)]^{2+}$ (**6**), was obtained as the product of the photolysis of **1** in a py:CH_3CN solvent mixture, showing the selective exchange of the CH_3CN ligand *trans* to phen. DFT calculations show that the lowest energy ^{1}MLCT and ^{3}MLCT states of **1′** are characterized by a decrease of electron density in a Ru−CH_3CN π-bonding orbital, thus weakening the bond to the CH_3CN ligand *trans* to phen. The promoted electron is localized on the LUMO with biq(π^*) character, strengthening the Ru−CH_3CN bond of the ligand positioned *trans* to biq. These results point at the direct role of the MLCT states in the photoinduced ligand exchange process. Our efforts could potentially serve as a route for the synthesis of heteroleptic inorganic complexes, as well as a new method for wavelength selective drug delivery in photochemotherapeutic applications.

ASSOCIATED CONTENT

Supporting Information

Additional crystal structure and crystallographic data, calculations, ^{1}H NMR data, emission spectra, and intermediate stability, and crystallographic information file. This material is available free of charge via the Internet at http://pubs.acs.org. CCDC numbers for structures herein: 957521, 957522. Crystallographic data can be obtained free of charge from The Cambridge Crystallographic Data Center via www.ccdc.cam.ac.uk/data_request/cif.

AUTHOR INFORMATION

Corresponding Author

*E-mail: turro@osu.edu.

Notes

The authors declare no competing financial interest.

ACKNOWLEDGMENTS

The authors thank the National Science Foundation (CHE-1213646) and the Ohio Supercomputer Center for partial support of this work. The authors are grateful to Dr. Judith C. Gallucci for aiding in the crystallographic work up.

REFERENCES

(1) Balzani, V.; Moggi, L. Photochemistry of coordination compounds: a glance at past, present, and future. *Coord. Chem. Rev.* **1990**, *97*, 313−326.

(2) Flamigni, L.; Barbieri, A.; Sabatini, C.; Ventura, B.; Barigelletti, F. Photochemistry and Photophysics of Coordination Compounds: Iridium. *Top. Curr. Chem.* **2007**, *281*, 143−203.

(3) Williams, J. A. G. Photochemistry and Photophysics of Coordination Compounds: Platinum − Excited States and Luminescence. *Top. Curr. Chem.* **2007**, *281*, 205−268.

(4) Campagna, S.; Puntoriero, F.; Nastasi, F.; Bergamini, G.; Balzani, V. Photochemistry and Photophysics of Coordination Compounds II. *Top. Curr. Chem.* **2007**, *280*, 117−214.

(5) Grätzel, M. Solar Energy Conversion by Dye-Sensitized Photovoltaic Cells. *Inorg. Chem.* **2005**, *44*, 6841.

(6) Rimmer, R. D.; Pierri, A. E.; Ford, P. C. Photochemically activated carbon monoxide release for biological targets. Toward developing air-stable photoCORMS labilized by visibile light. *Coord. Chem. Rev.* **2012**, *256*, 1509−1519.

(7) Pierri, A. E.; Pallaora, A.; Wu, G.; Ford, P. C A Luminescent and Biocompatible PhotoCORM. *J. Am. Chem. Soc.* **2012**, *134*, 18197−18200.

(8) Cline, E. D.; Adamson, S. E.; Bernhard, S. Homogenous Catalytic System for Photoinduced Hydrogen Production Utilizing Iridium and Rhodium Complexes. *Inorg. Chem.* **2008**, *47*, 10378−10388.

(9) Jasimuddin, S.; Yamada, T.; Fukuju, K.; Otsuki, J.; Sakai, K. Photocatalytic hydrogen production from water in self-assembled and supramolecular iridum-cobalt systems. *Chem. Commun.* **2010**, *46*, 8466−8468.

(10) Reece, S. Y.; Hamel, J. A.; Sung, K.; Jarvi, T. D.; Esswein, A. J.; Pijpers, J. J. H.; Nocera, D. G. Wireless Solar Water Splitting Using Silicon-Based Semiconductors and Earth-Abundant Catalysts. *Science* **2001**, *334*, 645.

(11) White, T. A.; Higgins, S. L. H.; Arachchige, S. M.; Brewer, K. J. Efficient Photocatalytic Hydrogen Production in a Single-Component System Using Ru,Rh,Ru Supramolecules Containing 4,7-Diphenyl-1, 10-Phenanthroline. *Angew. Chem., Int. Ed.* **2011**, *50*, 12209−12213.

(12) Pfennig, B. W.; Norris, M. R.; Zimmerman, N.; Gallagher, J. R.; McCloskey, A. I. Synthesis, spectroscopy, electrochemistry, and photochemistry of cyano-bridged mixed-valence coordination compounds containing two different types of intervalent charge-transfer bands. *Inorg. Chim. Acta* **2009**, *362*, 1701−1708.

(13) Burya, S. J.; Palmer, A. M.; Gallucci, J. C.; Turro, C. Photoinduced Ligand Exchange and Covalent DNA Binding by Two New Dirhodium Bis-Amidato Complexes. *Inorg. Chem.* **2012**, *51*, 11882−11890.

(14) Lutterman, D. A.; Fu, P. K.-L.; Turro, C. *cis*-$[Rh_2(\mu\text{-}O_2CCH_3)_2(CH_3CN)_6]^{2+}$ as a Photoactivated Cisplatin Analog. *J. Am. Chem. Soc.* **2006**, *128*, 738−739.

(15) Robson, K. C. D.; Koivisto, B. D.; Yella, A.; Sporinova, B.; Nazeeruddin, M. K.; Baumgartner, T.; Grätzel, M.; Berlinguette, C. P. Design and Development of Functionalized Cyclometalated Ruthenium Chromophores for Light Harvesting Applications. *Inorg. Chem.* **2011**, *50*, 5494−5508.

(16) Juris, A.; Balzani, V.; Barigelletti, F.; Campagna, S.; Belser, P.; Von Zelewsky, A. Ru(II) polypyridine complexes: photophysics, photochemistry, electrochemistry, and chemiluminescence. *Coord. Chem. Rev.* **1988**, *84*, 85−277.

(17) DelNegro, A. S.; Woessner, S. M.; Sullivan, P. B. Stereospecific, Unsymmetrical Photosubstituion in a Ligand-Bridged Dimer. *Inorg. Chem.* **2001**, *40*, 5056−5057.

(18) Sun, Y.; Joyce, L. E.; Dickson, N. M.; Turro, C. Efficient DNA photocleavage by $[Ru(bpy)_2(dppn)]^{2+}$ with visible light. *Chem. Commun.* **2010**, *46*, 2426−2428.

(19) Garner, R. N.; Gallucci, J. C.; Dunbar, K. R.; Turro, C. $[Ru(bpy)_2(5\text{-cyanouracil})_2]^{2+}$ as a potential light activated dual action therapeutic agent. *Inorg. Chem.* **2011**, *50*, 9213−9215.

(20) Respondek, T.; Garner, R. N.; Herroon, M. K.; Podgorski, I.; Turro, C.; Kodanko, J. J. Light activation of a cysteine protease inhibitor: Caging of a peptidomimetic nitrile with $Ru^{II}(bpy)_2$. *J. Am. Chem. Soc.* **2011**, *133*, 17164−17167.

(21) Singh, T. N.; Turro, C. Photoinitiated DNA binding by cis-$[Ru(bpy)_2(NH_3)_2]^{2+}$. *Inorg. Chem.* **2004**, *43*, 7260−7262.

(22) Sgambellone, M. A.; David, A.; Garner, R. N.; Dunbar, K. R.; Turro, C. Cellular toxicity induced by the photorelease of a caged bioctive molecule: Design of a potential dual-action Ru(II) complex. *J. Am. Chem. Soc.* **2013**, *135*, 11274−11282.

(23) Howerton, B. S; Heidary, D. K.; Glazer, E. C. Strained ruthenium complexes are potent light-activated anticancer agents. *J. Am. Chem. Soc.* **2012**, *134*, 8324−8327.

(24) Higgins, S. L. H.; Tucker, A. J.; Winkel, B. S. J.; Brewer, K. J. Metal to ligand charge transfer induced DNA photobinding in a Ru(II)-Pt(II) supramolecule using red light in the therapeutic window: a new mechanism for DNA modification. *Chem. Commun.* **2012**, *48*, 67−69.

(25) Ford, P. C. Properties and reactions of ruthenium(II) amine complexes. *Coord. Chem. Rev.* **1970**, *5*, 75−99.

(26) Ford, P. C. The ligand field photosubstitution reactions of d^6 hexacoordinate metal complexes. *Coord. Chem. Rev.* **1982**, *44*, 61−82.

(27) Ford, P. C.; Wink, D.; Dibenedetto, J. Mechanistic Aspects of the Photosubstitution and Photoisomerization reactions of d6Metal Complexes. *Prog. Inorg. Chem.* **1983**, *30*, 213−271.

(28) Malouf, G.; Ford, P. C. Photochemical reaction pathways of ruthenium(II) complexes. Evidence regarding the reactive excited state(s) from metal-to-ligand charge transfer excitation of pentaamine(pyridine)ruthenium(2+) and related complexes. *J. Am. Chem. Soc.* **1974**, *96*, 601−603.

(29) Malouf, G.; Ford, P. C. Photochemistry of the ruthenium(II) ammine complexes, $Ru(NH_3)_5(py\text{-}X)^{2+}$. Variation of systemic parameters to modify photochemical reactivities. *J. Am. Chem. Soc.* **1977**, *99*, 7213−7221.

(30) Durante, V. A.; Ford, P. C. Flash photolysis studies of ruthenium(II)-ammine complexes. 1. Transient intermediates in the photolysis of $Ru(NH_3)_5(py\text{-}X)^{2+}$ and their relationship to photosubstitution pathways. *Inorg. Chem.* **1979**, *18*, 588−593.

(31) Tfouni, E. Photochemical reactions of ammineruthenium(II) complexes. *Coord. Chem. Rev.* **2000**, *196*, 281−305.

(32) Martinez, M. S. Photochemical reactions of pentaammine(cyanopyridine)ruthenium(II) complexes, $[Ru(NH_3)_5L]^{2+}$. *J. Photochem. Photobiol., A* **1999**, *122*, 103−108.

(33) Pavanin, L. A.; da Rocha, Z. N.; Giesbrecht, E.; Tfouni, E. Photoaquation of cis-bis(azine)tetraammineruthenium(II) complexes, cis-$Ru(NH_3)_4(L)(L')^{n+1}$. *Inorg. Chem.* **1991**, *30*, 2185−2190.

(34) Sullivan, B. P.; Salmon, D. J.; Meyer, T. J. Mixed phosphine 2, 2′-bipyridine complexes of ruthenium. *Inorg. Chem.* **1978**, *17*, 3334−3341.

(35) Durham, B.; Walsh, J. L.; Carter, C. L.; Meyer, T. J. Synthetic applications of photosubstitution reactions of poly(pyridyl) complexes of ruthenium(II). *Inorg. Chem.* **1980**, *19*, 860−865.

(36) Caspar, J. V.; Meyer, T. J. Photochemistry of MLCT excited states. Effect of nonchromophoric ligand variations on photophysical properties in the series cis-$(bpy)_2L_2^{2+}$. *Inorg. Chem.* **1983**, *22*, 2444−2453.

(37) Durham, B.; Caspar, J. V.; Nagle, J. K.; Meyer, T. J. Photochemistry of tris(2,2′-bipyridine)ruthenium(2+) ion. *J. Am. Chem. Soc.* **1982**, *104*, 4803−4810.

(38) Allen, G. H.; White, R. P.; Rillema, D. P.; Meyer, T. J. Synthetic control of excited-state properties. Tris-chelate complexes containing the ligands 2,2′-bipyridine, and 2,2′-bipyrimidine. *J. Am. Chem. Soc.* **1984**, *106*, 2613−2620.

(39) Rillema, D. P.; Taghdiri, D. G.; Jones, D. S.; Keller, C. D.; Worl, L. A.; Meyer, T. J.; Levy, H. A. Structure and redox and photophysical properties of a series of ruthenium heterocycles based on the ligand 2,3-bis(2-pyridyl)qunoxaline. *Inorg. Chem.* **1987**, *26*, 578−585.

(40) Petroni, A.; Slep, L. D.; Etchenique, R. Ruthenium(II) 2,2′-Bipyridyl Tetrakis Acetonitrile Undergoes Selective Axial Photocleavage. *Inorg. Chem.* **2008**, *47*, 951.

(41) Liu, Y.; Turner, D. B.; Singh, T. N.; Angeles-Boza, A. M.; Chouai, A.; Dunbar, K. R.; Turro, C. Ultrafast Ligand Exchange: Detection of a Pentacoordinate Ru(II) Intermediate and Product Formation. *J. Am. Chem. Soc.* **2009**, *131*, 26−27.
(42) Krause, R. A. Synthesis of mixed complexes of ruthenium(II) with 2,2′-dipyridyl. *Inorg. Chim. Acta* **1977**, *22*, 209−213.
(43) Assefa, Z.; Stanbury, D. M. Oxidation of Coordinated Ammonia to Nitrosyl in the Reaction of Aqueous Chlorine with *cis*-$[Ru(bpy)_2(NH_3)_2]^{2+}$. *J. Am. Chem. Soc.* **1997**, *119*, 521−530.
(44) Kubow, S. A.; Marimon, M. E.; Takeuchi, K. J. Synthesis and characterization of oxoruthenium(IV) complexes that utilize a 2,2′-biquinoline ligand. *Inorg. Chem.* **1988**, *27*, 2761−2767.
(45) Bolger, J.; Gourdon, A.; Ishow, E.; Launay, J. P. Mononuclear and binuclear tetrapyrido[3,2-a:2′-3′-c:3″,2″-h:2‴,3‴-j]phenazine (tpphz) ruthenium and osmium complexes. *Inorg. Chem.* **1996**, *35*, 2937.
(46) Montalti, M.; Credi, A.; Prodi, L.; Gandolfi, M. T. *Handbook of Photochemistry*, 3rd ed.; Taylor & Francis Group: Boca Raton, FL, 2006; pp 601−616.
(47) Wegner, E. A.; Adamson, A. W. Photochemistry of complex ions. III. Absolute quantum yields for the photolysis of some aqueous chromium(III) complexes. Chemical actinometry in long wavelength visible region. *J. Am. Chem. Soc.* **1966**, *88*, 394−402.
(48) Otwinowski, Z.; Minor, W. Processing of X-ray Diffraction Data Collected in Oscillation Mode. *Methods in Enzymology, Vol. 276: Macromolecular Crystallography, Part A*; Academic Press: 1997.
(49) Sheldrick, G. A short history of *SHELX*. *Acta Crystallogr.* **2008**, *A64*, 112−122.
(50) Farrugia, L. WinGX Suite for Single Crystal Small Molecule Crystallography. *J. Appl. Crystallogr.* **1999**, *32*, 837−838.
(51) *International Tables for Crystallography, Vol. C*; Kluwer Academic Publishers: Dordrecht, The Netherlands, 1992.
(52) Frisch, M. J.; Trucks, G. W.; Schlegel, H. B.; Scuseria, G. E.; Robb, M. A.; Cheeseman, J. R.; Scalmani, G.; Barone, V.; Mennucci, B.; Petersson, G. A.; et al. *Gaussian 09*, revision A.1; Gaussian, Inc.: Wallingford, CT, 2009.
(53) Becke, A. D. Density-functional exchange-energy approximation with correct asymptotic behavior. *Phys. Rev.* **1988**, *38*, 3098−3100.
(54) Becke, A. D. Density-functional thermochemistry. III. The role of exact exchange. *J. Chem. Phys.* **1993**, *98*, 5648−5652.
(55) Lee, C.; Yang, W.; Parr, R. G. Development of the Colle-Salvetti correlation-energy formula into a functional of electron density. *Phys. Rev. B: Condens. Matter Mater. Phys.* **1988**, *37*, 785−789.
(56) Hehre, W. J.; Radom, L.; Chleyer, P. V.; Pople, J. A. *Ab initio Molecular Orbital Theory*; John Wiley & Sons: New York, 1986.
(57) Andrae, D.; Haussermann, U.; Dolg, M.; Stoll, H.; Preuss, H. Energy-adjusted *ab initio* pseudopotentials for the second and third row transition elements. *Theor. Chim. Acta* **1990**, *77*, 123−141.
(58) Dennington, R., II; Keith, T.; Millam, J. *GaussView 3*; Semichem, Inc.: Shawnee Mission, KS, 2007.
(59) Fantacci, S.; Angelis, F. D.; Selloni, A. J. Absorption spectrum and solvatochromism of the $[Ru(4,4'\text{-COOH-}2,2'\text{-bpy})_2(NCS)_2]$ molecular dye by time dependent density functional theory. *J. Am. Chem. Soc.* **2003**, *125*, 4381−4387.
(60) Klassen, D. M. Excited states of mixed ligand complexes of ruthenium(II) with 2-(2′pyridyl)quinoline and 2,2′-biquinoline. *Chem. Phys. Lett.* **1982**, *93*, 383−386.
(61) Bonneson, P.; Walsh, J. L.; Pennington, W. T.; Cordes, A. W.; Durham, B. Six-coordinate complexes with 1, 10-phenathroline ligands in the trans configuration. Preparation of trans-bis(1, 10-phenanthroline)ruthenium(II) complexes and crystals structure of trans-bis(1, 10-phenanthroline)bis(pyridine)ruthenium(II) hexafluorophosphate. *Inorg. Chem.* **1983**, *22*, 1761−1765.
(62) Bolletta, F.; Vitale, M. Electrochemiluminescence quantum yield of some Ru(II) polypyridine complexes. *Inorg. Chim. Acta* **1990**, *175*, 127−131.
(63) Turki, M.; Daniel, C.; Zalis, S.; Vlcek, A., Jr.; Van Slageren, J.; Stufkens, D. J. UV-Visible Absorption Spectra of $[Ru(E)(E')(CO)_2(iPR\text{-}DAB)]$ (E = E′= $SNPH_3$ or Cl; E = $SnPH_3$ or Cl, E′ = CH_3; iPR-DAB = N,N′-Di-isopropyl-1,4-diaza-1,3-butadiene): Combination of CASSCF/CASPT2 and TD-DFT Calculations. *J. Am. Chem. Soc.* **2001**, *123*, 11431−11440.
(64) Kirgan, R. A.; Sullivan, B. P.; Rillema, D. P. Photochemistry and Photophysics of Coordination Compounds: Rhenium. *Top. Curr. Chem.* **2007**, *281*, 45.
(65) Lin, Z.; Hall, M. B. Electron density analysis of the transition states of substitution reactions of 17- and 18-electron hexacarbonyl complexes. *J. Am. Chem. Soc.* **1992**, *114*, 6574−6575.
(66) Lin, Z.; Hall, M. B. Theoretical studies of inorganic and organometallic reaction mechanisms. 5. Substitution reactions of 17- and 18-electron transition metal hexacarbonyl complexes. *Inorg. Chem.* **1992**, *31*, 2791−2797.
(67) De Vito, D.; Sidorenkova, H.; Rotzinger, F. P.; Weber, J.; Merbach, A. E. Can Octahedral t_{2g}^6 Complexes Substitute Associatevly? The Case of Isoelectonic Ruthenium(II) and Rhodium-(III) Hexaaquaions. *Inorg. Chem.* **2000**, *39*, 5547−5552.
(68) Bahreman, A.; Limburg, B.; Siegler, M. A.; Bouwman, E.; Bonnet, S. Spontaneous Formation in the Dark, and Visible Light-Induced Cleavage, of a Ru-S Bond in Water: A Thermodynamic and Kinetic Study. *Inorg. Chem.* **2013**, *52*, 9456−9469.